# Scanning Tunnelling Spectroscopy & Microscopy

Report by Jelle Dionot
Practical done with Marcel Brändlein, under the supervision of Nadine Witkowski

*Université Pierre et Marie Curie*
*Institut des Nanosciences de Paris*

Nanomat Master Program – Group 2
Friday, December 9th 2011

# Contents

# Introduction

Only thirty years ago, G. Binning, H. Rohrer et al. reported the first observation of the quantum mechanical tunnelling current through vacuum[1]. Based on this effect, experimental set-ups were elaborated to measure the small variations of current and therefore probe the electronic density of a material surface, giving birth to the so-called scanning tunnelling microscopy (STM). Even though this technique can be very cumbersome to master finely, it is about to reach a state-of-the-art in such a way that atomic resolution and functional observations can quite easily be done. In this report, we present the basic principles of this technique and the analysis of the interface between an $MoS_2$ monocrystal surface covered by 8CB liquid crystal and a model for the adsorption geometry of this organic compound on the hexagonal substrate, based on the study of the obtained STM images.

# 1 Basic principles

## 1.1 Theoretical background

Considering free electrons as plane waves $\psi$ propagating along the $z$-direction, quantum mechanics predict that in the presence of a uniform, finite but infinitely long step potential $V_0$, the plane waves are non-zero into the barrier, which is unexpected from a classical point of view. The electron wavefunction inside the potential barrier is indeed exponentially damped as it propagates, such that:

$$\psi(z) = A \cdot T \cdot \mathrm{e}^{-\kappa z} \qquad \text{with} \qquad \kappa = \sqrt{\frac{2m(V_0 - E)}{\hbar^2}} \tag{1}$$

In the above equation, T is the transmission coefficient and A is a normalization constant. For $z$ going to infinity, the wavefunction is damped down to zero. But for a potential barrier of finite thickness $d$, electrons with kinetic energy smaller than $V_0$ can still and all overcome the barrier, depending on the thickness. Indeed, two metallic planes separated by a small distance $d = z_2 - z_1$ can represent such a described system, in which the gap between the plates represent the potential barrier. This potential $V_0(z)$ varies along $z$. Using the WKB[2] approximation method, Schrödinger equation is solved giving the following transmission coefficient for a particle tunnelling through a single potential barrier characterized by the so-called turning points $z_1$ and $z_2$:

$$T \simeq \exp\left(-2\int_{z_1}^{z_2} \kappa(z)\mathrm{d}z\right) \tag{2}$$

According to the Landauer-Büttiker formalism, the transmission coefficient is related to the tunnelling current such that the latter is proportional to the sum over all the transmission channels. However, in order to achieve a net current along one direction, a potential bias $V_{\text{bias}}$ is applied so that the potential is higher on one side of the gap. The obtained tunnelling current reads:

$$I = \frac{e}{\pi\hbar}\int_{E_F}^{E_F + eV_{\text{bias}}} T(E,d)\mathrm{d}E \tag{3}$$

[1] G. Binning, H. Rohrer, Ch. Gerber, E. Weibel, Appl. Phys. Lett. 40, 178 (1982)
[2] Wentzel–Kramers–Brillouin

In this equation, one sees that firstly the tunnelling current and the distance between the two plates are coupled, and secondly it depends on the applied bias voltage. Furthermore, perturbation theory calculations can show that the derivative of the tunnelling current with respect to the applied bias is a function of the *local density of states* (*LDOS*) $\rho$ at the surface of the metal, such that:

$$\frac{\mathrm{d}I(V)}{\mathrm{d}V} \propto \rho(\mathbf{r}, E_\mathrm{F} + eV) \tag{4}$$

The local density of states $\rho$ is directly proportional to the atomic charge distribution and therefore the measure of the derivative of the tunnelling current gives great insight on the atoms occupying the probed surface.

## 1.2 Experimental aspects

In practice, STM requires a metallic tip ideally sharp enough to be ended by a single atom, which represent half of the conductive material required for the tunnelling current to occur, the sample being the second half. An image of the surface is made thanks to a scanning of the tip on the surface, measuring the local density of states as expressed in equation 4. The resolution of the measurement depends on the quality of the tip. In our experiment, we use a $Pt_{90}Ir_{10}$ wire of a fraction of a millimetre thick, which we cut at grazing angle with a pair of blunt scissors which literally rips a rather sharp tip off the wire. Platinum makes the tip extremely inert and resistant to corrosion and Iridium provides stiffness for high sharpness. Such technique, when done correctly, provides similar results and resolution as compared to a tip made by chemical etching of tungsten.

Based on the above theoretical aspects, tunnelling current is nowadays mainly manipulated within three experimental techniques. An STM image can be acquired through *constant height* method (*CHM*), *constant current* method (*CCM*) and numerous information can be extracted from so-called *scanning tunnelling spectroscopy* (*STS*). Equation 4 displays the physical quantities involved in the latter mentioned technique, which consists in measuring the LDOS by measuring the variation of the current with respect to the tuned bias voltage or change in the distance between tip and sample. CHM and CCM are rather used for topography purposes, since they allow to map the LDOS of the probed surface, respectively by keeping the distance (height) between the tip and the sample constant and thus measuring variations of tunnelling current; and by keeping the tunnelling current constant at a *set point* value $I_\mathrm{t}$ thanks to a feedback adjustment process which constantly readjusts the distance between the tip and the sample to counterbalance the change of tunnelling current which originates from the variation of the probed LDOS. This feedback loop is monitored by a *proportional-integral* (*PI*) *controller*. The difference between the set point of tunnelling current and, on the one hand, the actual measured value at each position (proportional gain); and on the other hand, an integrated value of all tunnelling current in the image (integral gain), is amplified and used to provide higher sensitivity of the probing system. The aim of this practical is to cover two methods, namely CCM and STS, in order to present STM images as well as qualitative studies of different type of materials.

In our experiment, STM images of *highly oriented pyrolytic graphite (HOPG)* are obtained by CCM and then treated. On the other hand, the materials studied in STS are

gold (Au), molybdenum disulphide ($MoS_2$) and HOPG which are respectively a metal, a semiconductor and a semimetal. Here, one focuses on the dependence of the tunnelling current with the applied bias and the distance between the tip and the sample, $I(V)$ and $I(z)$ respectively.

The samples consists in small film held on a metallic holder of typical size 1 cm, the whole being horizontally magnetically attached to the STM set-ups *easyScan 2 STM* from *nanosurf*. The tip comes horizontally perpendicularly to the sample and must be firstly approached by hand. Thereafter, piezoelectric nanopositioners are controlled by a the STM software for a fine approach at a typical distance of a few nanometres. The tip is brought closer to the sample by very small steps, each time the software checking if tunnelling current is felt. If not, the tip is retracted a bit and the sample is approached slightly. The tip makes a step again, on a safe distance, until tunnelling current is measured.

# 2 Scanning Tunnelling Spectroscopy

## 2.1 Height dependence of the tunnelling current

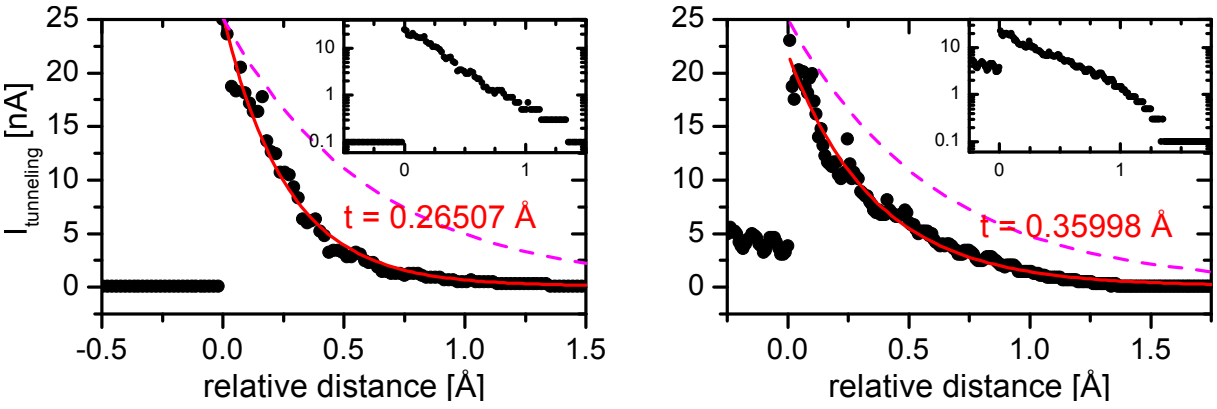


**(a)** *Single STS acquisition* **(b)** *Four averaged STS acquisitions*

**Figure 1:** *Tunnelling current as a function of height $I(z)$ from: one STS measurement on the left and 4 averaged STS acquisitions on the right. Acquired data are the black dots whereas a fit consisting in $e^{-z/t}$ is presented in red, with the corresponding characteristic length $t$. The dashed pink line comes from literature values.*

Our first set of measurements consisted in acquiring tunnelling current over HOPG with increasing the distance from the tip to the sample $z$. Figure 1 depicts the measured tunnelling current as a function of the set distances. The software used allows to set a safe value of tunnelling current. If half of this value is overcome by the absolute value of the measured tunnelling current, the measurement would stop in order to prevent the tip from crashing onto the sample. Also, the distance scale is set in such a way that we could extract a relative scale as presented in the figures 1a and 1b. The observed behaviour of the tunnelling current is clearly an exponential decay. The insets on each graph show a rather straight line as it is a semilog representation. Figure 1a corresponds to a single STS measurement whereas figure 1b presents 4 STS acquisitions which were averaged. The exponentially decaying function used to fit the data shows two rather distinct characteristic decay lengths $t$. Moreover, figure 1b presents a non-zero tunnelling

current below the 0 value of the relative distance, where in principle it should be zero. Indeed, we believe that some impurities have impinged on the tip in such a way that tunnelling current can be felt at even smaller distances. Besides, even though the fitting can be rather well achieved, we observe an important disagreement with literature values from which the pink lines have been generated. However, this observations does not prevent us from trying to estimate some physical quantities of our samples. Together with equation 2, equation 3, giving the tunnelling current, may allow us to express the exponential dependence as follows:

$$I(z) \propto \mathrm{e}^{-z\cdot\sqrt{\frac{2m\Phi}{\hbar^2}}} \Rightarrow \frac{1}{t} = \sqrt{\frac{2m\Phi}{\hbar^2}} \tag{5}$$

In the above relation, $\Phi$ stands for the potential containing both the workfunction of the tip and the one of the sample. It further writes:

$$\Phi = \frac{\hbar^2}{2m}\frac{1}{t^2} \tag{6}$$

Using the characteristic lengths resulting in the fitting of the data presented in figure 1, one obtains:

$$\Phi^{(a)} = 54.23 \text{ eV} \qquad \Phi^{(b)} = 29.40 \text{ eV}$$

Literature values[3] of the workfunction of HOPG gives $\Phi_{\text{HOPG}} = 4.6$ eV and for the $Pt_{90}Ir_{10}$ tip, we find[4] $\Phi_{\text{tip}} = 5.65$ eV. We observe a non-negligible disagreement with tabulated values although our result belongs to the same order of magnitude. The discrepancy might be explained by either contamination of the tip which may have altered the tunnelling current measurements, or to an improvable calibration of the set-up, mainly the piezoelectric machinery which provides ultimately the scale in $z$ values. At least the exponential decaying can really well be observed.

The same type of study has been made on a gold sample. Figure 2 depicts the corresponding measurements, as before, showing the tunnelling current with respect to the tip-sample distance. Firstly, besides the apparent exponential decay observed on figure 2a, two additional peaks are present a relative distance 6 Å and 7.5 Å. These two peaks could be collected various time, allowing us to think that the sample or the tip have been contaminated by atoms ripped off from the earlier measurements leading to additional tunnelling current signals, distinct from the one of currently studied gold. To emphasize this statement, a technique of cleaning of the sample has been applied, thanks to a relatively high bias voltage imposed for a few seconds. At such high bias voltage, the tip tend to attract and is able to rip off atoms from the sample surface, due to an overlap of the tip and the sample potential. Together with agility and patience, this technique could enable to move away some atoms on the surface, mainly the contaminating ones. Figure 2b shows the acquisition following the above described "cleaning" procedure and the two additional peaks seem to undergo a shifting towards lower relative distance values. This shows that this technique has a true impact on contaminating species and gives good hope to get rid of them if repeated wisely.

Based on figure 2a, the exponentially decaying behaviour gives a characteristic decay length $t$ such that the total workfunction found is $\Phi = 9.04$ eV. Compared to literature

[3] F. Maeda, T. Takahashi, H. Ohsawa, S. Suzuki, Phys. Rev. B 37, 4482 (1988)

[4] http://environmentalchemistry.com/yogi/periodic/Pt.html

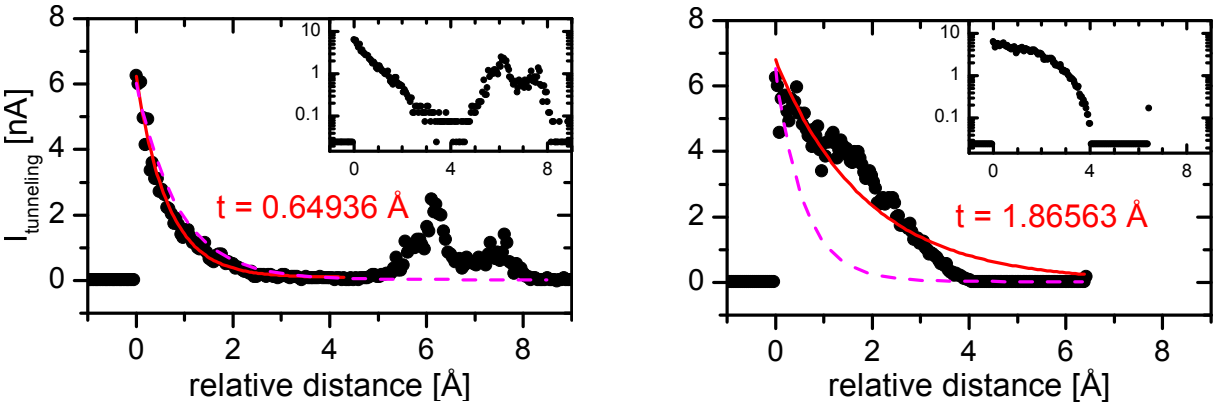


**(a)** *Single STS acquisition* **(b)** *Single STS acquisition after treatment*

**Figure 2:** *Tunnelling current as a function of height $I(z)$ from single STS acquisitions over gold. The acquisition presented on the right-hand-side graph has been made after some cleaning of the tip (see the text). Acquired data are the black dots whereas a fit consisting in $e^{-z/t}$ is presented in red, with the corresponding characteristic length $t$. The dashed pink line comes from literature values.*

value[5] which gives $\Phi^{\ell} = \Phi_{\text{Au}} + \Phi_{\text{tip}} = 10.74$ eV, one obtains good results.

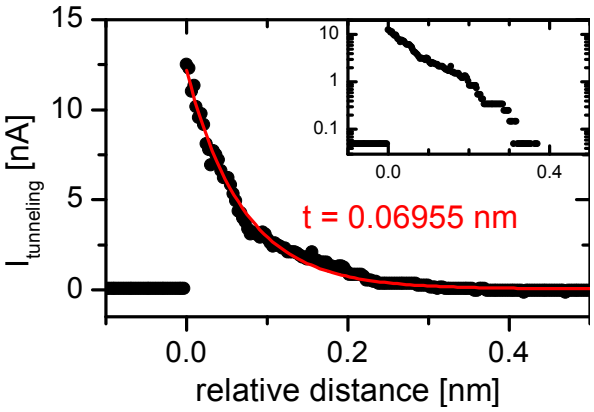


**Figure 3:** *Tunnelling current as a function of height $I(z)$ from single STS acquisitions over $MoS_2$. Acquired data are the black dots whereas a fit consisting in $e^{-z/t}$ is presented in red, with the corresponding characteristic length $t$.*

Ultimately, the dependence of the tunnelling current with respect to the height have been investigated with the molybdenum disulphide $MoS_2$ sample. The exponentially decaying behaviour of $I(z)$ is well obtained and the total workfunction calculated from equation 6 gives $\Phi = 7.876$ eV. Subtracting the value of the workfunction of the tip, one estimates the workfunction of this sample as $\Phi_{MoS_2} = 2.226$ eV which we can not compare to any found literature value unfortunately.

## 2.2 Voltage dependence of the tunnelling current

This second section deals with the study of the variation of tunnelling current with respect to changes of the applied bias voltage. In such STS experiments, the distance between

[5] http://environmentalchemistry.com/yogi/periodic/Au.html

the tip and the sample is primarily set and the voltage is tuned in a predefined range of values (usually centred on zero), therefore the current goes from tip to sample and from sample to tip within each scan.

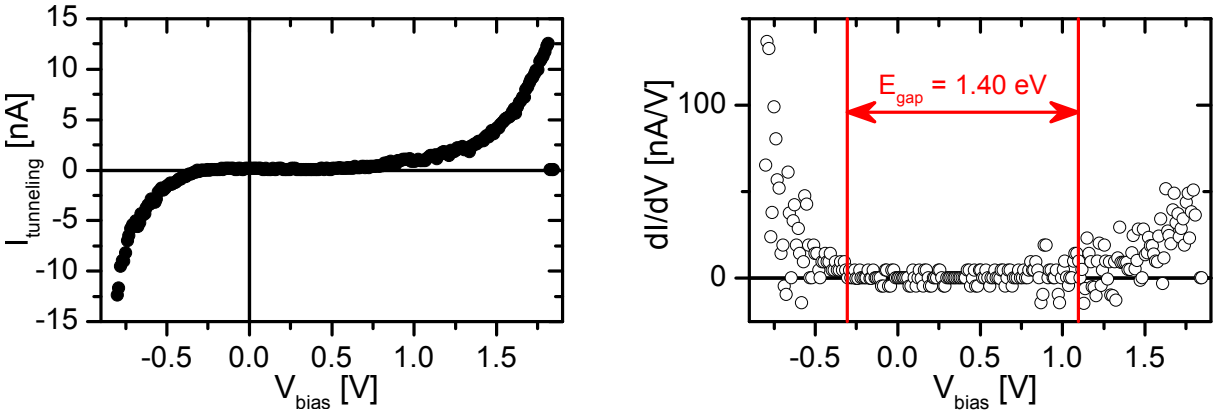


**(a)** $I(V)$ *from* $-1.0$ *to* $2.0$ V **(b)** $\mathrm{d}I/\mathrm{d}V$ *from* $-1.0$ *to* $2.0$ V

**Figure 4:** *Tunnelling current as a function of applied bias* $I(V)$ *from single STS acquisitions over* $MoS_2$*. Acquired data are the full black circles on the left and are used for the calculation of* $\mathrm{d}I/\mathrm{d}V$ *depicted on the right as empty circles.*

Firstly, one studies the behaviour of the tunnelling current with respect to the applied bias on our molybdenum disulphide sample. Figure 4 depicts the measured tunnelling current (grap 4a) together with its derivative (graph 4b) with respect to the applied bias voltage $V$. One observes that $I(V)$ shows symmetry with respect to a certain value of the bias $V$. The symmetry illustrates the fact that the current can run from tip to surface and reversely from surface to tip. The observation that it is not centred around zero bias may originate from the fact that the tip and the sample have very different chemical potential. Indeed, the charge carriers excited either from the tip to the surface or from the surface to the tip require different excitation energy to be removed from their material. Besides this observed symmetry, one sees that the tunnelling current is zero for a certain range of applied bias. Here, this is interpreted in such a way that the electrons have to undergo a sufficient potential in order to tunnel from the surface to the tip. This behaviour of the charge carriers is characteristic to semiconductor materials, where the LDOS is expected to be zero at the surface since the chemical potential lies in the energy gap, and the electrons lying in the valence band require sufficient energy to excite into the conduction and thereafter possibly tunnel to the tip. Figure 4b indeed illustrates this energy gap and a value of $E_{\mathrm{gap}}^{\mathrm{MoS_2}} = 1.40$ eV is found and falls in rather good agreement with literature values[6] giving a gap of about 1.8 eV.

Our interest then focuses on the gold sample. Figure 5 shows singly the tunnelling current with respect to the applied bias. A linear behaviour of the current is exhibited and the data are thereof fitted. As a matter of fact, this behaviour is somewhat expected since gold is a metal, and it is quite likely that we can observe it. It indeed follows the Ohm's law and the conductance of gold can therefore be extracted. It is shown on the figure and we hence the ohmic resistance of gold is estimated at $R = 40.10$ MΩ.

Lastly, one likewise focuses on HOPG and the influence of a tuned bias on the tunnelling current. Figure 6 schemes the measured tunnelling current (graph 6a) along with

[6] Y. Youngki, G. Kartik, S. Sayeef, Nano Lett. 11, 3768 (2011)

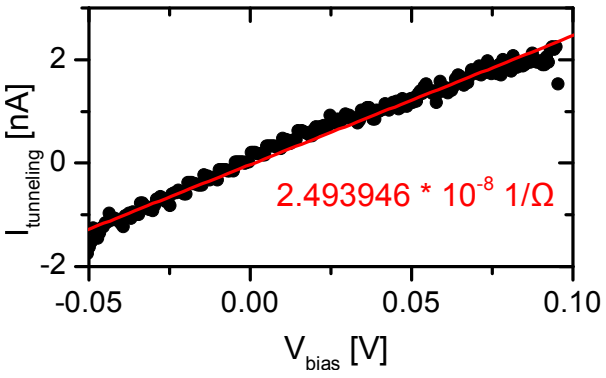


**Figure 5:** *Tunnelling current as a function of applied bias $I(V)$ from a single STS acquisition over gold. The red line stands for a linear fit underneath which the value of the gold ohmic resistance is displayed.*

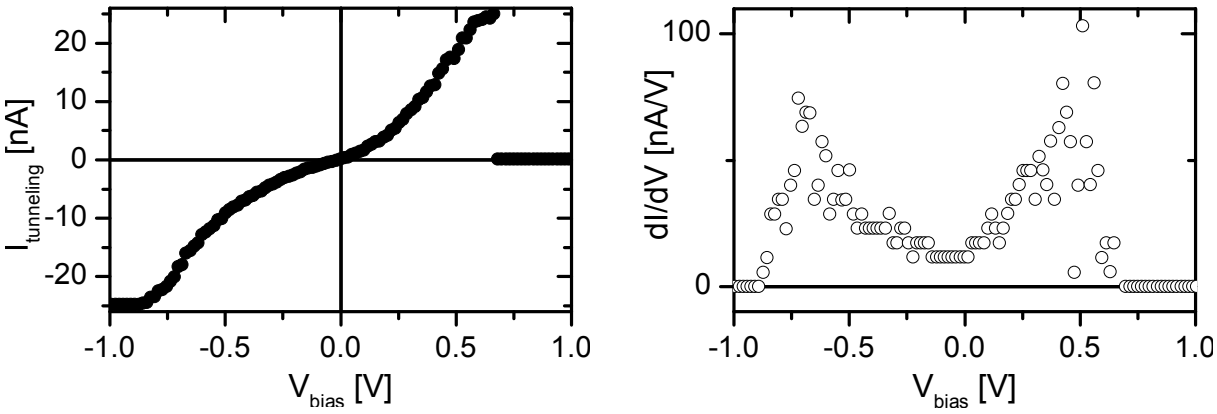


**(a)** $I(V)$ *from* $-1.0$ *to* $1.0$ V

**(b)** $\mathrm{d}I/\mathrm{d}V$ *from* $-1.0$ *to* $1.0$ V

**Figure 6:** *Tunnelling current as a function of applied bias $I(V)$ from a single STS acquisition over HOPG. Acquired data are the full black circles on the left and are used for the calculation of $\mathrm{d}I/\mathrm{d}V$ depicted on the right as empty circles.*

its derivative (graph 6b) with respect to the applied bias $V$. At low voltage, one sees that the current is slightly linear as for our gold sample, but still it is non-zero as it was the case for the semiconductor $MoS_2$. This is emphasized on its derivative representation, where the curve is flat but lying at a non-zero value for voltage close to 0. Moreover, the range of applied bias is large enough to observe a current behaviour analogous to the semiconductor: at low voltage, the current varies slowly, without ever cancelling. This phenomenon reflects the fact that the carriers require very low potential energy for tunnelling current to occur, and moreover there seem to have always available carriers for this current. Indeed, this is characteristic of semimetal where there is a very small overlap between the top of the valance band and the bottom of the conduction band. Also, as shown in figure 6b, the LDOS is constant in the vicinity of small bias. Two-dimensional electron systems are described by a constant LDOS. Graphite is the superimposition of graphene layers, which are 2D electron systems. Therefore, one can believe that at low bias, the probed states are those of the outermost layer of the graphite sample, which is a graphene layer with dangling bonds. For increasing bias (in absolute value), the tunnelling current reaches a maximum and then drops down rapidly (better observed in figure 6b). This is indeed the signature of a parabolic density of states characteristic of

systems with a linear dispersion relation as it is the case of graphene for low energies in the vicinity of the high symmetry points of its two-dimensional hexagonal Brillouin zone.

# 3 Scanning Tunnelling Microscopy

In spite of our cautiousness and involvement, our recorded STM images have been damaged when exported. Also, despite our cordial request to the members of group 1 who worked with us, or rather in the same room as us the day of our experiment, no collaboration could be made. The following data presented are those kindly provided by group 3[7], acquired on the HOPG sample. Added with descriptions of these data, we will discuss as well what we observed during our experiment, based on our notes, even though we do not have the corresponding images to display.

## 3.1 STM of HOPG

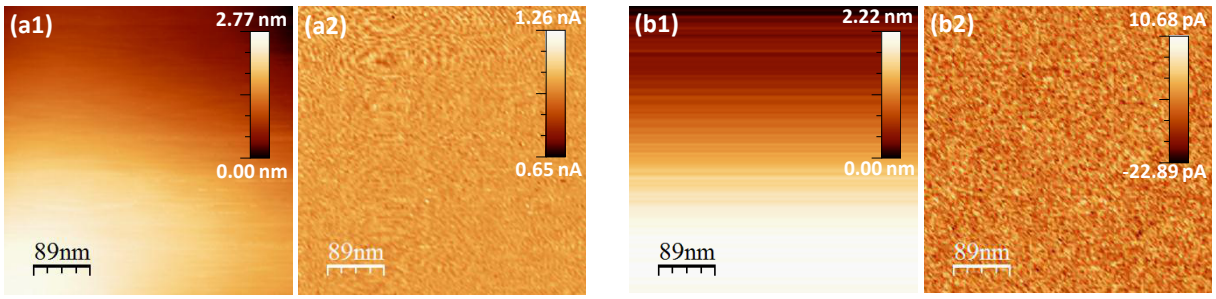


**(a)** *Left to right scan (forward)* **(b)** *Right to left scan (backward)*

**Figure 7:** *STM images of HOPG obtained in CCM in forward and backward scan. On each figure, the left picture is the topographic image and the right on is the corresponding tunnelling current map.*

Figures 7a and 7b depict STM topographic images ($7a_1$ and $7b_1$) together with the corresponding tunnelling current maps ($7a_2$ and $7b_2$), for two different scanning directions: forward and backward respectively. The topographic images show a continuous gradient of intensity from bright to dark orange. According to the scanning direction, the direction of this gradient differs. This gradient can be due to a net drift of the sample originating from thermal motions and ambient vibrations. This drift gets lower and lower with time as the whole STM system reaches a state of equilibrium, the piezoelectric machinery together with the PI controller being stabilized. In figure $7b_2$, the observed lines are parallel to the gradient, which is a coincidence. Indeed, two features can be distinguished: the observed stripes on both topographic images which are a signature of a step-like surface and various slopes of these lines which originate from thermal effects. These features are not clearly visible on the presented pictures in figure 7 but could be observed experimentally. To go further, when we looked at the tunnelling current maps, we could see some fringes that we can actually see in figure $7a_1$. They are interference patterns and originate from the wave nature of the probed electrons. The previously mentioned features that are not visible on the presented pictures concern the stripes that could be observed in both topographic and tunnelling current images. Also, the contrast

[7]Philipp Ehrenreich and Shabnam Hashemi Dolatabadi, group 3, Nanomat M2 2011

in the tunnelling current maps was opposite from a forward scan to a backward scan. This could be interpreted as and effect due to the surface type made of steps separating stacked layers. When the tip goes toward a increasing step, the tunnelling current between the tip and the sample reaches a maximum before the PI controller has the time to readjust the height of the tip climbind the step. On the contrary, when the scanning tip is about to go down a step, the current reaches a minimum when the feedback loop adjusts the height. These two cases gave different contrasts according to the direction of the scan with respect to the direction of "stairs" formed by the steps (whether the stairs goes up or down). Interferences, drift as well as contrast depending on the direction of the scan makes STM images' interpretation rather tricky.

## 3.2 Influence of the integral gain on the contrast

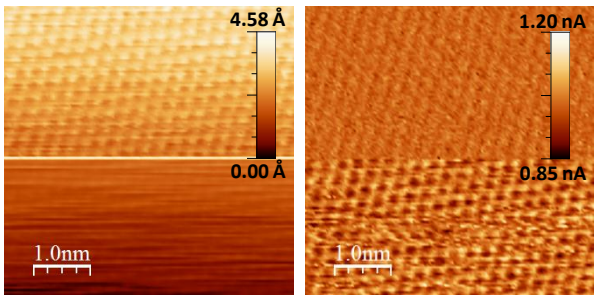


**Figure 8:** *STM topographic image of HOPG and its tunnelling current map. The upper parts of the pictures correspond to a scan with an integral gain* $G_{\mathrm{I}} = 100$ *while the lower parts were obtained after changing the gain to* $G_{\mathrm{I}} = 4000$ *during the scan.*

In figure 8, we present the influence of a change in the integral gain of the PI controller. Again, topographic images are shown along the pictures of the corresponding tunnelling current, in a window of $5 \times 5$ nm$^2$. The gain has been multiplied by 40 from the upper images to obtain what is depicted beneath. We can see that the contrast in topographic images showing, for small gain, a patterned surface, is lost at higher gain where one drift and tilt can be guessed. With a higher gain, the PI controller needs more time to adjust at each step, and therefore the system becomes less sensitive to change in height as the scan progresses. On the contrary, the current map shows an opposite tendency. A patterned surface is clearly observed as the contrast between high and low tunnelling current values is enhanced. Therefore, the variation of LDOS is well observed for high integral gain and a judicious value can be kept for further scans in order to improve the resolution of topographic images.

## 3.3 Data treatments and quantitative example

The topographic images can be treated with the software WsXM[8] in order to considerably improve the contrast and enhanced the quality of the STM images. A *parabolic flattening* has been applied to images presented in figure 9, providing a remove of the non-linear background as well as and overall increase of the patterned surface contrast. In order to preserve the step-like properties of the image, one could have use a *local plane fit* instead.

[8] I. Horcas et al., Rev. Sci. Instrum. 78, 013705 (2007)

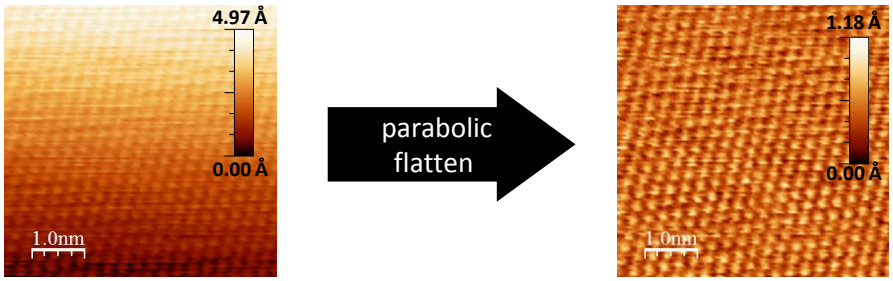


**Figure 9:** *STM image of HOPG obtained in CCM before and after a parabolic flattening treatment.*

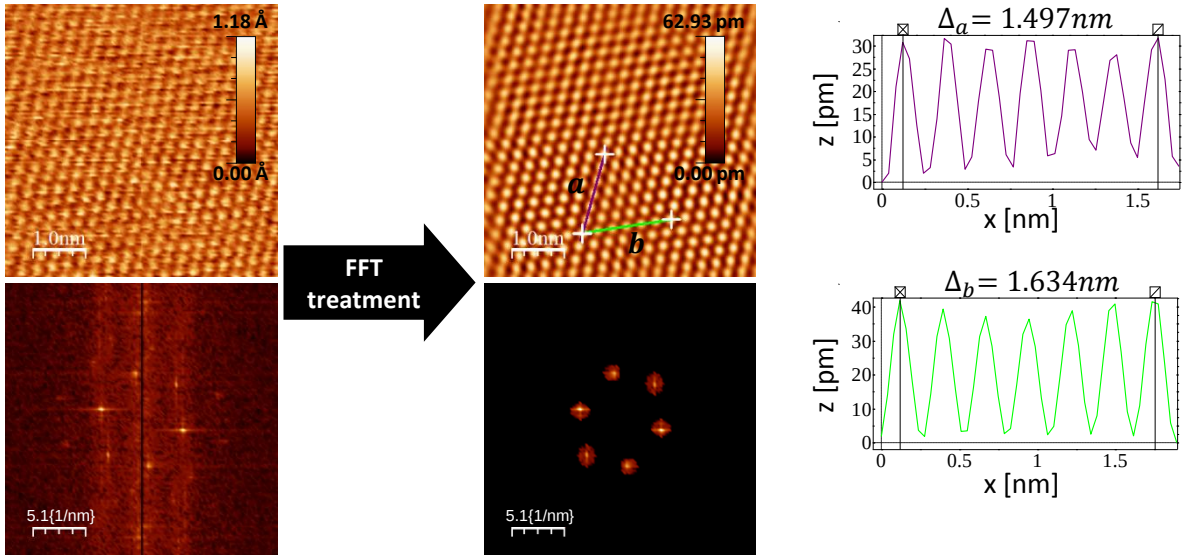


**Figure 10:** *STM images of HOPG obtained in CCM and parabolic flattened before and after a Fast Fourier Transform treatment. The upper parts of the pictures show the topographic images whereas the lower parts depict the corresponding FFT images. One notices the apparent hexagonal symmetry in Fourier space, analogous to the hexagonal Brillouin zone of graphene. On the right-hand-side, the plot profile of the corresponding coloured lines depicted in the treated image.*

Above all the various direct image treatments that WsXM is able to do on the STM images, a very subtle technique is proposed and presented in this work. Especially for patterned structure and images showing periodicity, this technique starts from a two-dimensional Fast Fourier Transform of an STM image. Figure 10 presents the use of this method. The probed sample being graphite, the structure expected to be observed should be patterned. The decomposition of graphene structure in Fourier space leads to a structure with hexagonal symmetry as schemed in the picture on the bottom-left-hand corner the figure. Therefore, selecting the very first orders decompositions in the Fourier space and cancelling the rest of this reciprocal image gives should theoretically give the patterned structure in direct space with a very good contrast. This is what we actually can do and it is shown on the treated images in figure 10. The maxima of intensity in the treated topographic image are at regular position as expected. A close look is given at these bright dots with the measurement of their periodicity along two apparently favoured directions. The repeated distances between directions $a$ and $b$ are obtained by averaging

over 7 points:

$$d_a = 0.214 \text{ nm} \qquad d_b = 0.233 \text{ nm}$$

The two above values should be the same given the underlying symmetry and their difference can be assigned to the fact that the sample surface may not be perfectly perpendicular to the tip. But these experimental values are rather close to the lattice constant of HOPG $a_{\text{HOPG}} = 2.4612$ Å. The above described technique using FFT and how it has been used focuses mainly in improving the resolution and mainly the contrast to get images of good quality. Higher orders Fourier components could have been kept in order to refine the generated image. But in order to visually measure a lattice constant, it seems to be well adapted.

# Conclusion

From a purely quantum mechanical effect that is the tunnelling current, we have seen that very practical applications and quite stunning results can be obtained in a rather quick and reasonably reproducible way. Spectroscopy as well as microscopy give great insight on the electronic behaviour and the structure of various material, with the limit that these materials must be able to conduct a current. Having hints on the molecular arrangements on a surface and given the subnanometric resolution, we could also assess quantitatively the lattice constant of graphene. Scanning tunnelling techniques are of major importance in the development of our knowledge of matter at such a scale and given its fast evolution, may become a state-of-the-art technique over the next years.